Soliton electro-optic effects in paraelectrics

Eugenio DelRe and Mario Tamburrini

Fondazione Ugo Bordoni, Via B. Castiglione 59, 00142 Rome, Italy, and
Instituto Nazionale Fisica della Materia, Unitá di Roma I, Italy

Aharon J. Agranat

Department of Applied Physics, Hebrew University of Jerusalem, Jerusalem 91904, Israel

The combination of charge separation induced by the formation of a single photorefractive screening soliton and an applied external bias field in a paraelectric is shown to lead to a family of useful electro-optic guiding patterns and properties.   © 2000 Optical Society of America
    OCIS codes: 190.5330, 230.2090.

Apart from their inherent interest as particular products of nonlinearity, spatial solitons hold the promise of making optical steering in bulk environments feasible.[1,2] Photorefractive screening solitons differ from other known manifestations of spatial self-trapping in that they are particularly easy to observe and versatile,[3] and recent experiments with photorefractive strontium barium niobate and potassium niobate have demonstrated two conceptual applications of the guiding properties of these solitons.   In the first case, a tunable directional coupler was realized that makes use of two independent slab solitons[4]; in the second, it was observed that self-induced phase matching enhanced second-harmonic generation.[5] Although these results suggest a means of obtaining all-optical functionality, actual implementation is hampered by a generally slow nonlinear response,[6] which can be accelerated only at the expense of stringent intensity requirements.[7] In contrast, nondynamic guiding structures have been observed by fixing of a screening soliton[8] or in relation to the observation of spontaneous self-trapping during a structural crystal phase transition.[9] One possible method of obtaining acceptable dynamics is to make direct use of the electro-optic properties of the ferroelectrics involved, in combination with the internal photorefractive space-charge field deposited by the soliton. Since photorefractive charge activation is wavelength dependent, one can induce charge separation in solitonlike structures at one active wavelength (typically visible) and then read the electro-optic index modulation at a different, nonphotorefractive, wavelength (typically infrared).[10,11] For noncentrosymmetric samples (such as the above-mentioned crystals) that typically host screening-soliton formation, the electro-optic refractive-index modulation is proportional to the static crystal polarization **P** and thus to the electric field (linear electro-optic effect). For these samples no electro-optic modulation effects are possible: For whatever value of external constant electric field E_{ext}, the original soliton-supporting guiding pattern remains unchanged. In centrosymmetrics, such as photorefractive potassium lithium tantalate niobate,

solitons are supported by the quadratic electro-optic effect.[12–15] In this case the nonlinear combination of the internal photorefractive field with an external electric field can give rise to new and useful soliton-based electro-optic phenomena, which we study here for what is believed to be the first time.

The basic mechanism leading to screening-soliton formation is the following: A highly diffracting optical beam ionizes impurities hosted in the lattice of an electro-optic crystal. An externally applied electric field makes these mobile charges drift to less-illuminated regions, forming a double layer that reduces the resultant electric field in the illuminated region. For an appropriate electro-optic sample this reduction leads to self-lensing and soliton propagation when beam diffraction is exactly compensated for. For slab solitons, i.e., those self-trapped beams that originate from a beam that linearly diffracts in only one transverse dimension (x), for a given soliton intensity FWHM Δx, a given ratio between the soliton peak intensity and the (generally artificial) background illumination (intensity ratio), $u_0{}^2 = I_{peak}/I_b$, solitons form for a particular value of applied external biasing field $\bar{E}$. The soliton-supporting electric field E is expressed as $E = (V/L)[1 + I(x)/I_b]^{-1}$, where V is the external applied voltage, L is the distance between the crystal electrodes (thus, $\bar{E} = V/L$), and $I(x)$ is the optical intensity of the soliton, confined in the transverse (x) dimension.[12] This electric field, which is the result of a complex nonlinear light–matter interaction, is present even when the generating optical field is blocked and the sample is illuminated with a nonphotorefractively active light. Charge separation is smeared out only by slow recombination associated with dark conductivity and is characterized by considerably long decay times. The nonphotorefractively active illumination, although it does not lead to any further evolution of the internal charge field, will be affected by the index inhomogeneity, owing to the quadratic electro-optic response described by the relation $\Delta n = -(1/2)n^3 g_{eff} \epsilon_0{}^2 (\epsilon_r - 1)^2 E^2$, where n is the refractive index of the crystal, g_{eff} is the effective electro-optic coefficient for a given

scalar configuration, ϵ_0 is the vacuum dielectric constant, and ϵ_r is the relative dielectric constant. The actual electric field in the crystal is now $E = (V/L)[1 + I(x)/I_b]^{-1} - (V/L) + E_{ext}$, where E_{ext} (in general, $\neq \bar{E}$) is the externally applied electric field after the nonlinear processes have occurred (the readout field). The index pattern that is induced is

$$\Delta n = -\Delta n_0 \left[\frac{1}{1 + I(x)/I_b} - 1 + \frac{E_{ext}}{V/L} \right]^2, \qquad (1)$$

where $\Delta n_0 = (1/2)n^3 g_{eff} \epsilon_0^2 (\epsilon_r - 1)^2 (V/L)^2$. In Fig. 1 we show two families of induced index patterns associated with two solitons at different saturation levels. In Fig. 1(a), a 7-μm FWHM soliton at wavelength $\lambda = 514$ nm ($\Delta n_0 \simeq 5.4 \times 10^{-4}$, for $n = 2.45$) with an intensity ratio $u_0^2 = 4$ leads to three characteristic pattern regimes: For $\eta = E_{ext}/(V/L) \simeq 1$, a soliton-supporting potential is formed. For $\eta \simeq 0$, an anti-guiding hump appears, whereas for intermediate values of η, a twin-waveguide potential forms. Analogous results can be predicted for the strongly saturated regime shown in Fig. 1(b), in which an 11-μm soliton is formed for $u_0^2 \simeq 22$.

Experiments are carried out with an apparatus that has been well documented in the literature.[13,14] An enlarged TEM$_{00}$ Gaussian beam from a cw argon-ion laser operating at $\lambda = 514$ nm is focused by an $f = 150$ mm cylindrical lens onto the input facet of a $3.7^{(x)}$ mm $\times 4.6^{(y)}$ mm $\times 2.4^{(z)}$ mm sample of zero-cut paraelectric potatssium lithium tantalate niobate at $T = 20\,°C$ (with a critical temperature $T_c = 11\,°C$), giving rise to an approximately one-dimensional x-polarized Gaussian beam of $\Delta x \cong 11 \ \mu$m (a soliton beam), and the entire crystal is illuminated with a second, homogeneous beam (a background beam) from the same laser, polarized along the y axis. The focused and the plane-wave beams copropagate along the z direction. A constant voltage V is applied along the crystal's x direction; the crystal itself is doped with vanadium and copper impurities and is photorefractively active at the laser wavelength. Guiding patterns can be investigated either by illumination of the crystal with an infrared beam (as mentioned above) or simply by use of the same soliton-forming wavelength but at a lower intensity, since the photorefractive temporal dynamics are proportional to the beam intensity. Here we use this readout method, and in what follows all read–write experiments are at $\lambda = 514$ nm, with $I_{write}/I_{read} \cong 20$. By changing the value of the applied readout voltage, V_{ext}, we can explore the optical potential described by Eq. (1) through the variable η. Beam distribution is investigated by imaging of the facets of the sample onto a CCD camera by means of a second lens placed after the sample (along the z direction).

In Fig. 2 the observation of a single photorefractive screening soliton is shown. The 11-μm soliton, whose intensity distribution is shown at the input facet in Fig. 2(a) and whose output self-trapped distribution is shown in Fig. 2(c), has an intensity ratio $u_0^2 \cong 22$ at $V_{exp} = 1.33$ kV, annulling linear diffraction to 24 μm, as shown in Fig. 2(b).

Soliton formation takes approximately 3 min, for $I_{peak} \simeq 1.8$ kW/m^2 ($I_b \simeq 80$ W/m^2), measured directly before the sample, meaning that erasure during readout would take, at the very least, $\sim$1 h (i.e., longer than any of our experiments). Had we used an infrared readout beam, decay would have been halted indefinitely. Given the sample values $g_{eff} = 0.12$ m^4 C^{-2}, $\epsilon_r \simeq 9000$, and $\Delta n_0 \simeq 6.9 \times 10^{-4}$, the expected value of soliton formation would be $V_{th} \simeq 1.27$ kV.

In Fig. 3 we show the same region of the crystal in Fig. 2 illuminated by a less-intense read beam (but that is otherwise identical to the soliton-generating beam) at various values of η. For $\eta = 1$ the output beam is identical to the soliton (apart from the actual intensity). For low values of η ($\eta < 0.4$) the index pattern given by Eq. (1) is antiguiding, and the output beam is scattered and split into two diffracting beams [this is referred to as beam bursting; see Fig. 1(b)]. As η is increased, the defocusing is weakened, and for $\eta \approx 0.45$ the sample gives rise to beam splitting of the twin-waveguide structure formed by the two-hump
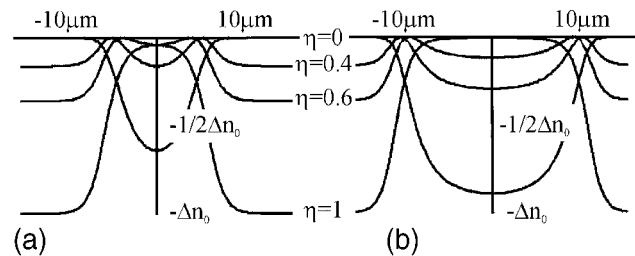

Fig. 1. Predicted electro-optic index patterns resulting from the soliton-deposited space-charge field for (a) $u_0 = 2$ and (b) $u_0 = 4.7$.
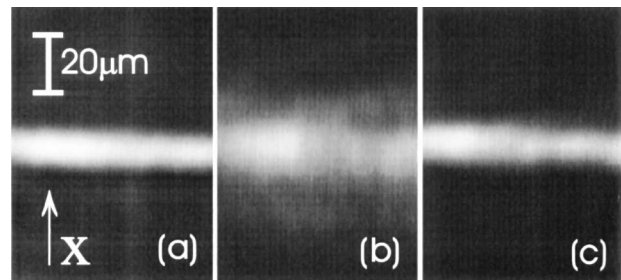

Fig. 2. Soliton formation: (a) intensity distribution of an 11-μm beam before it enters the crystal; (b) 24-μm diffracted intensity distribution at the output facet, after the beam has undergone linear propagation ($V = 0$) in the sample; (c) self-trapped output facet distribution for $V_{exp} = 1.33$ kV at $T = 20\,°C$ for $u_0 \simeq 4.7$.
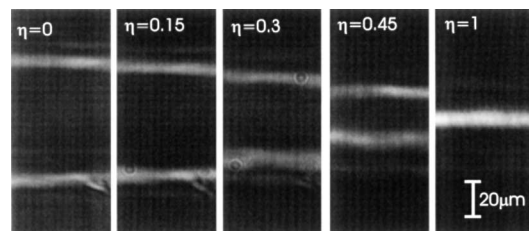

Fig. 3. Output light distribution of the readout beam. For $\eta = 0$–0.3 the beam is scattered. For $\eta = 0.45$ a twin-beam structure forms, whereas for $\eta = 1$ the original guiding pattern emerges.
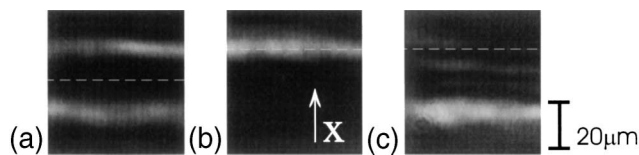
Fig. 4 Electro-optic switching: (a) output light distribution of the read beam for $\eta = 0.45$; (b) side-guided beam, when the crystal is shifted 10 μm in the negative x direction, launching the read beam in the direction of the top twin waveguide; (c) output in the same condition but $\eta = 0.8$. The dashed lines indicate the position of the input beam axis.
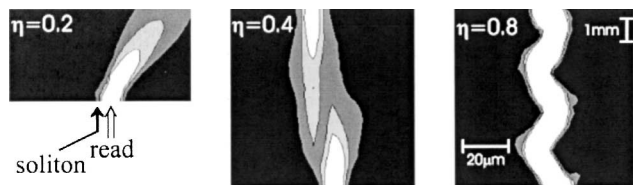

Fig. 5. Predicted evolution of an ≈ 7-μm beam: (a) top view of readout in an 8-mm sample for $\eta = 0.2$ (beam deflection and diffraction), (b) one-beat directional coupling for $\eta = 0.4$ from right hump to left hump, (c) mode beating for $\eta = 0.8$ ($\approx$2-mm mode beat).

potential, as shown in Fig. 1. The distance between the two beams is ≈ 20 μm. As opposed to the previous defocusing case, in this case light is exciting a guided mode.

Next we shift the crystal in the x direction with respect to the optical beam to launch the beam directly into one of the twin guides for intermediate values of η. For $\eta = 0.45$, when the crystal is shifted by 10 μm, the beam is guided by the side hump, as shown in Fig. 4(b). In this forward-guiding condition, we change η from 0.45 to 0.8. The index structure changes from a double-hump twin waveguide to a single guiding pattern (see Fig. 1). The optical beam is redirected as shown in Fig. 4(c).

It is therefore possible to realize, by the formation of a single photorefractive centrosymmetric screening soliton, three qualitatively different optical circuits: a single waveguide, a double-waveguide beam splitter, and an antiguiding beam stopper. If we shift the crystal to launch the guided beam into one of the twin guides, it is possible to change the direction of the beam while maintaining its strong confinement, allowing us to realize an electro-optic switch. Had we used a longer sample, launching the beam in a twin waveguide would have led to a tunable directional coupler, as shown in Fig. 5.

The observed phenomena represent an important step in the achievement of feasible soliton-based components in two major respects. The first is that the observed phenomena occur with the formation of a single soliton that is used only to deposit a pattern of charge displacement (a particular volume hologram), whereas switching from one regime to the other occurs only through a change of the applied electric field. Thus switching dynamics are limited only by capacity-charging times, as in all other electro-optic devices. Second, whereas screening-soliton formation requires a constant applied external field during readout, the use of independent electrodes can allow the formation of composite circuitry in cascade, all from a single soliton.

References

1. G. I. Stegeman and M. Segev, Science **286,** 1518 (1999).
2. M. Segev and G. I. Stegeman, Phys. Today **51**(8), 42 (1998).
3. B. Crosignani, P. Di Porto, M. Segev, G. Salamo, and A. Yariv, Riv. Nuovo Cimento **21,** 1 (1998).
4. S. Lan, E. DelRe, Z. Chen, M. Shih, and M. Segev, Opt. Lett. **24,** 475 (1999).
5. S. Lan, M. Shih, G. Mizell, J. A. Giordmaine, Z. Chen, C. Anastassiou, J. Martin, and M. Segev, Opt. Lett. **24,** 1145 (1999).
6. L. Solymar, D. J. Webb, and A. Grunnet-Jepsen, *The Physics and Applications of Photorefractive Materials* (Clarendon, Oxford, 1996).
7. K. Kos, G. Salamo, and M. Segev, Opt. Lett. **23,** 1001 (1998).
8. M. Klotz, H. Meng, G. J. Salamo, M. Segev, and S. R. Montgomery, Opt. Lett. **24,** 77 (1999).
9. E. DelRe, M. Tamburrini, M. Segev, R. Della Pergola, and A. J. Agranat, Phys. Rev. Lett. **83,** 1954 (1999).
10. M. Shih, Z. Chen, M. Mitchell, M. Segev, H. Lee, R. S. Feigelson, and J. P. Wilde, J. Opt. Soc. Am. B **14,** 3091 (1997).
11. For linear schemes based on screening, see A. Bekker, A. Ped'el, N. K. Berger, M. Horowitz, and B. Fischer Appl. Phys. Lett. **72,** 3121 (1998); Ph. Dittrich, G. Montemezzani, P. Bernasconi, and P. Gunter, Opt. Lett. **24,** 1508 (1999).
12. M. Segev and A. J. Agranat, Opt. Lett. **22,** 1299 (1997).
13. E. DelRe, B. Crosignani, M. Tamburrini, M. Segev, M. Mitchell, E. Refaeli, and A. J. Agranat, Opt. Lett. **23,** 421 (1998).
14. E. DelRe, M. Tamburrini, M. Segev, E. Refaeli, and A. J. Agranat, Appl. Phys. Lett. **73,** 16 (1998).
15. A. J. Agranat, R. Hofmeister, and A. Yariv, Opt. Lett. **17,** 713 (1992).